JOURNAL OF THERMOPHYSICS AND HEAT TRANSFER
Vol. 14, No. 2, April–June 2000

Effects of the Centrifugal Forces on a Gas Between Rotating Cylinders

L. M. de Socio,* N. Ianiro,† and L. Marino‡
University of Rome "La Sapienza," 00161 Rome, Italy

The gas flow between two concentric rotating cylinders is investigated over a wide range of governing dimensionless products. Analytic solutions are given for the free molecular flow, for the Bhatnagar–Gross–Krook model up to the first-order approximation, and for the hydrodynamic limit in the Chapman–Enskog expansion. The slip flow boundary conditions are extensively discussed, and a constructive solution to the transitional flow is proposed. Numerical direct simulation data are obtained and adopted as exact reference experimental results.

Nomenclature

c	= sound speed
f	= molecular velocity distribution function
Gr	= $\Delta R/R_1$
Kn	= Knudsen number
N	= number of representative molecules
N_s	= number of time steps
n	= number density
r, θ, z	= cylindrical coordinates
T	= temperature
u_θ	= tangential velocity
v_r, v_θ, v_z	= component of microscopic velocity $\boldsymbol{v}$
ΔR	= gap width
Θ	= ratio of wall temperatures
κ	= thermal conductivity
λ	= mean free path
μ	= viscosity coefficient
ρ	= mass density
Ω	= angular speed

Subscripts

0	= condition at rest
1, 2	= internal and external wall, respectively

Introduction

THE subject of this paper is the Couette flow between two concentric rotating cylinders with radii R_1 and $R_2 > R_1$. This problem has received noticeable attention in the past, and the pertinent literature is extremely vast and increasing due to the interest in this physical situation, where mass forces act on the fluid.[1–4]

The problem is considered in the entire Knudsen number range to take into account rarefaction effects in addition to geometric and wall velocity parameters. The analytical and numerical solutions obtained are aimed at providing better physical insight into the relevance of each parameter in establishing steady flow field characteristics.

Recently direct simulation obtained by numerical codes[5] has provided reference solutions that proved to be in excellent agreement with the unfortunately scarce experimental data. We adopted a code based on the direct-simulation Monte Carlo (DSMC) method to obtain what we will consider in the following as the database of exact solutions.

The main significant dimensionless products on which the considered phenomenology depends are the Knudsen number Kn_0, the Mach numbers at the two walls Ma_1 and Ma_2, the temperature ratio $\Theta = T_2/T_1$, and the ratio of the gap width to the internal radius $Gr = \Delta R/R_1$. Here $Kn_0 = \lambda_0/\Delta R$ and $Ma = \Omega R/c$ and λ_0 is the mean free path of the fluid at rest, ΩR is the wall velocity, Ω is the angular speed, c is the speed of sound at the wall temperature, and T is the temperature. The indices 1 and 2 refer to the internal and the external wall, respectively.

The limit cases for $Kn_0 \to 0$ and $Kn_0 \to \infty$ will be considered first. In particular when the Knudsen number tends to zero, the hydrodynamic limit of the Boltzmann equation will be formally expressed in the form of the Navier–Stokes (NS) equations and the associated boundary conditions in the usual linear slip flow form.

A further approximation of the boundary conditions for small Knudsen number Kn_0, such as Burnett's approximation, was not considered due to the cumbersome calculations that are involved and to the still debated usefulness and physical derivation.[6,7]

For $Kn_0 \to \infty$, the free molecular flow (FMF) solution and the solution to the linearized Bhatnagar–Gross–Krook (BGK) model up to first order will be given. As a by-product, the value of the velocity slip at the walls will be shown as a function of the set of dimensionless products reported earlier.

Comparisons of the results of the analytical models presented previously are given with respect with the exact simulated ones in a number of cases. Finally, attention will be paid to the particular case where $\Theta = 1$, $Ma_2 = 0$, and $Ma_1 \neq 0$. In this case, and in the transitional regime, for fixed Gr, fluid flow situations are present where the density distribution along the gap follows the NS model in a region adjacent to the exterior wall and FMF behavior near the internal wall. Approximate solutions for the density and the velocity will then be proposed that compare favorably with the exact solutions.

Direct Simulation

As mentioned, we will take the results of a direct simulation using a DSMC as exact reference data. Previous research[5] showed substantial agreement between simulated and experimental data, although the available experiments were relatively old and some of them, for high Knudsen number Kn_0, are ambiguous.[2]

Our calculations were carried out by running a computer code (on a personal computer Pentium II, 200 MHz) that was adapted from one presented in Ref. 8. In all of the cases the gas was argon, the physical properties of which are reported in Ref. 8, the computational domain was divided into 100 cells with $N = 10{,}000$ representative particles. The convergence was proved by a criterion based on the norm $(g^i - g^{i-1})/g^{i-1}$, where g^i is the value of a

Received 4 June 1999; revision received 8 September 1999; accepted for publication 9 September 1999.

*Professor, Dip. Meccanica e Aeronautica, Via Eudossiana 18. Member AIAA.

†Associate Professor, Dip. Metodi e Modelli Matematici per le Scienze Applicate, Via A, Scarpa 16; ianiro@dmmm.uniroma1.it.

‡Research Scientist, Dip. Metodi e Modelli Matematici per le Scienze Applicate, Via A, Scarpa 16; marino@dmmm.uniroma1.it.

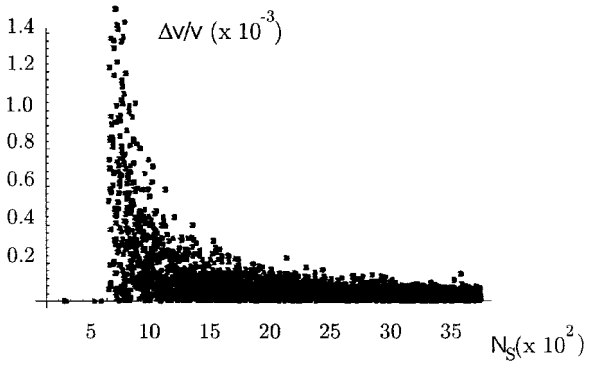

a) $N = 1000$; 100 cells

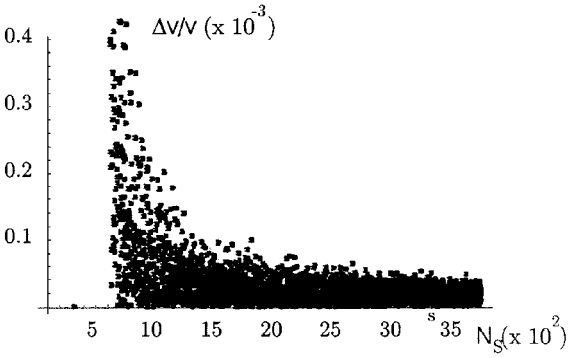

b) $N = 10{,}000$; 100 cells

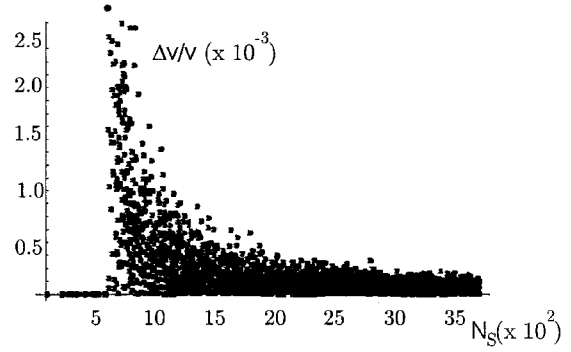

c) $N = 10{,}000$; 500 cells

Fig. 1 Case $\Theta = 1$, $Kn_0 = 2$, $Ma_1 = 0.5$, $Gr = 0.1$.

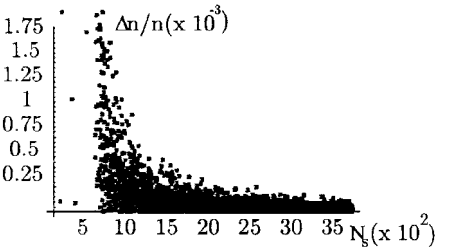

a) $N = 1000$; 100 cells

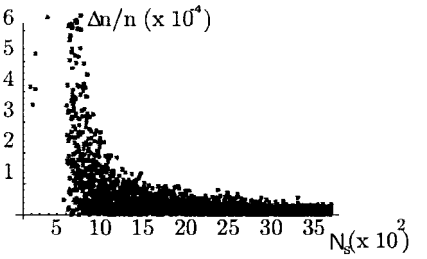

b) $N = 10{,}000$; 100 cells

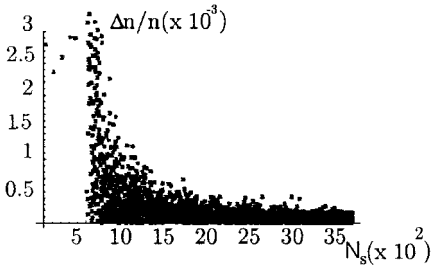

c) $N = 10{,}000$; 500 cells

Fig. 2 Case $\Theta = 1$, $Kn_0 = 2$, $Ma_1 = 0.5$, $Gr = 0.1$.

macroscopic variable (density, temperature, velocity) at step i in some indicative cells.

No attempt was made in optimizing the CPU time, and some runs took a few days to reach accurate results. The most critical cases required $N_s = 4000$ time steps, each time step Δt being constant. We recall that Δt is an updating step in a process that is stationary.[8]

Figures 1 and 2 show the convergence of the velocity modulus and number density to the final result in a significant case as a function of the number of steps. In Figs. 1 and 2, $\Delta u/u = (u^i - u^{i-1})/u^{i-1}$ was calculated in the midstep cell and is analogous for the number density n.

NS Equations

The gas is confined between two coaxial isothermal cylinders infinitely long so that the properties of the gas do not change along the cylinder axis z. By taking into account the axial symmetry, the distribution function does not depend on the angular θ coordinate. It follows that the stationary Boltzmann equation in rescaled macroscopic cylindrical coordinates, as usual, reads

$$Df = v_r \frac{\partial f}{\partial r} + \frac{v_\theta^2}{r}\frac{\partial f}{\partial v_r} - \frac{v_r v_\theta}{r}\frac{\partial f}{\partial v_\theta} = \frac{1}{Kn_0} Q(f, f) \qquad (1)$$

where Q is the usual Boltzmann collision operator, $\boldsymbol{v} = (v_r, v_\theta, v_z)$ is the velocity of a particle, and $r \in [R_1, R_2]$.

The boundary conditions at $r = R_1, R_2$, corresponding to zero mass flux at the walls, are diffusive, that is,

$$f(R_1, \boldsymbol{v}) = -M_1(\boldsymbol{v}) \int_{v_r < 0} \mathrm{d}\boldsymbol{v} v_r f(R_1, \boldsymbol{v}), \qquad v_r > 0 \quad (2a)$$

$$f(R_2, \boldsymbol{v}) = M_2(\boldsymbol{v}) \int_{v_r > 0} \mathrm{d}\boldsymbol{v} v_r f(R_2, \boldsymbol{v}), \qquad v_r < 0 \quad (2b)$$

with $M_i = \exp\{-[v_r^2 + (v_\theta - \Omega_i R_i)^2 + v_z^2]/2kT_i\}/(2\pi k^2 T_i^2)$, where k is the ratio of the Boltzmann constant to the molecular mass.

At small $Kn_0 = \epsilon$, we can construct a solution to the boundary value problem of Eqs. (1) and (2) of the form

$$f^\epsilon = f_0 + \epsilon f_1 + \cdots + \epsilon f_B + f_E$$

The first terms are the interior solutions given by the Chapman–Enskog expansion, f_B is the boundary-layer expansion, and f_E is the error term. Here f_0 is a Maxwellian distribution whose macroscopic parameters satisfy the NS equations ($u_r = 0, \ \forall r$)

$$\frac{\partial}{\partial r}(\rho k T) = \frac{1}{r}\rho u_\theta^2 \qquad (3a)$$

$$\frac{\partial}{\partial r}\left[r^2 \mu \left(\frac{\partial u_\theta}{\partial r} - \frac{u_\theta}{r}\right)\right] = 0 \qquad (3b)$$

$$\frac{\partial}{\partial r}\left[r\kappa \frac{\partial T}{\partial r}\right] + 2\mu\left[\frac{\partial u_\theta}{\partial r} - \frac{u_\theta}{r}\right]^2 = 0 \qquad (3c)$$

under no velocity slip and no temperature jump boundary conditions,

$$u_\theta(R_i) = \Omega_i R_i, \qquad T(R_i) = T_i, \qquad i = 1, 2$$

where $\mu(T)$ and $\kappa(T)$ are the viscosity and the thermal conductivity coefficients and the total mass

$$\int_{R_1}^{R_2} r\rho(r)\,\mathrm{d}r$$

is assigned.

In the following, the derivation of Eqs. (3) from Eq. (1) is formally proven, and Eq. (3) is solved for constant μ and κ, taking into account the boundary slip conditions that come from f_B.

Far from the boundaries, the solution is $f^\epsilon = f_0 + \epsilon f_1 + \epsilon^2 f_2 + \cdots$ with $f_0, f_1, f_2, \ldots$, such that

$$\begin{aligned} Q(f_0, f_0) &= 0 \\ Df_0 &= 2Q(f_0, f_1) = Lf_1 \\ Df_1 &= 2Q(f_0, f_2) + Q(f_1, f_1) \\ &\cdots \end{aligned} \tag{4}$$

where f_0 is a Maxwellian distribution and $f_1 = L^{-1}(Df_0) + \Psi_1$ provided that $\mathcal{P}Df_0 = 0$, where $\mathcal{P}$ is the projection onto the null $L = \mathrm{span}\{1, \boldsymbol{v}, v^2\}$, and Ψ_1 is an arbitrary function belonging to null L (Refs. 9–11).

From $\mathcal{P}Df_0 = 0$ one has

$$\frac{1}{r}\frac{\partial}{\partial r}(r\rho u_r) = 0, \qquad \frac{\partial}{\partial r}(\rho kT) = \frac{\rho u_\theta^2}{r} \tag{5}$$

The first of Eqs. (5) with the boundary conditions gives $u_r = 0$, $\forall r$.

Next

$$f_1 = L^{-1}\left[v_r\frac{(v_\theta - u_\theta)}{kT}\right] f_0\left[\frac{\partial u_\theta}{\partial r} - \frac{u_\theta}{r}\right] + L^{-1}\left\{v_r\left[\frac{v_r^2 + (v_\theta - u_\theta)^2}{2kT} - \frac{5}{2}\right]\right\} f_0\frac{1}{T}\frac{\partial T}{\partial r} + \Psi_1 \tag{6}$$

and the solvability condition to obtain f_2 gives Eqs. (3b) and (3c) with

$$\mu = \frac{1}{kT}\int \mathrm{d}\boldsymbol{v} v_r(v_\theta - u_\theta)L^{-1}[v_r(v_\theta - u_\theta)]f_0$$

$$\kappa = \frac{1}{T}\int \mathrm{d}\boldsymbol{v} v_r v^2 L^{-1}\left\{v_r\left[\frac{v_r^2 + (v_\theta - u_\theta)^2}{2kT} - \frac{5}{2}\right]\right\} f_0$$

In the $T_1 = T_2$ case and for small values of the Mach number at the walls, the temperature T does not significantly change with r, so that μ and κ can be assumed constant. Then analytical solutions can be obtained for the NS equations with no-slip boundary conditions. In particular for the tangential velocity and the density distribution, one has

$$u_\theta(r) = \frac{c_1 r}{2} + \frac{c_2}{r}, \qquad \rho(r) = \rho_0 \exp\left[\int h_2(r)\,\mathrm{d}r\right]$$

where

$$h_2(r) = \frac{h_1(r) - T'(r)}{T(r)}, \qquad h_1(r) = \frac{c_1^2}{4r} + \frac{c_2^2}{r^3} + \frac{c_1 c_2}{r}$$

with $c_1 = 2(\Omega_1 R_1^2 - \Omega_2 R_2^2)/(R_1^2 - R_2^2)$ and $c_2 = [R_1^2 R_2^2(\Omega_2 - \Omega_1)]/(R_1^2 - R_2^2)$, and which is analogous for $T(r)$.

The expressions for the macroscopic variables hold in the interior of the domain but not at its boundaries. The boundary-layer expansion f_B provides the transition, over a distance ϵ, from the boundary conditions imposed at $r = R_1$, R_2 to the Chapman–Enskog expansion.[9,10]

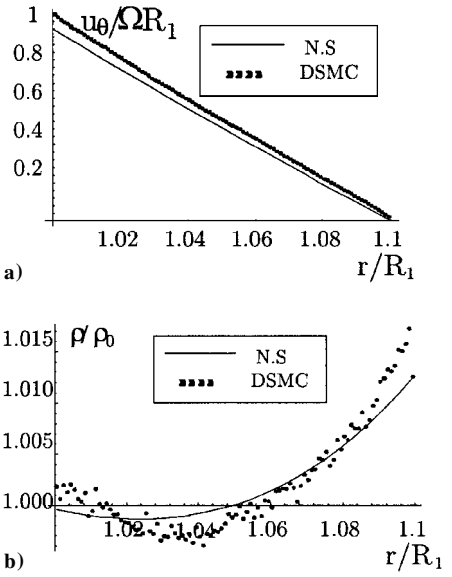

Fig. 3 Comparison of DSMC results with the analytical NS results: no-slip BC, $\Theta = 1$, $Kn_0 = 0.002$, $Ma_1 = 0.5$, and $Gr = 0.1$.

The slip boundary conditions that come from the boundary-layer terms are[11,12]

$$\begin{aligned} u_\theta(R_1) &= \Omega_1 R_1 + \sigma\lambda\left(\frac{\mathrm{d}u_\theta}{\mathrm{d}r} - \frac{u_\theta}{r}\right)_{R_1} \\ u_\theta(R_2) &= \Omega_2 R_2 - \sigma\lambda\left(\frac{\mathrm{d}u_\theta}{\mathrm{d}r} - \frac{u_\theta}{r}\right)_{R_2} \end{aligned} \tag{7}$$

whereas the temperature jump is negligible for $\Theta = 1$.

Figures 3a and 3b show, in a significant case, the comparison and the excellent agreement between the previous solutions and the DSMC solutions as far as velocity and density are concerned. The corresponding temperature profiles (not shown) show negligible differences.

FMF

At large Knudsen numbers, the Boltzmann equation for FMF takes the form

$$v_r\frac{\partial f}{\partial r} + \frac{v_\theta^2}{r}\frac{\partial f}{\partial v_r} - \frac{v_r v_\theta}{r}\frac{\partial f}{\partial v_\theta} = 0 \tag{8}$$

with the boundary conditions already given in Eq. (2).

The distribution function f is constant along the straight lines

$$v_\theta = \mathrm{const}/r, \qquad v_r^2 + v_\theta^2 = 2E \tag{9}$$

$$f(r, \boldsymbol{v}) = -J_1 M_1[\boldsymbol{v}(R_1)]H\left[v_r - (\sqrt{r^2 - R_1^2}/R_1)|v_\theta|\right] + J_2 M_2[\boldsymbol{v}(R_2)]H\left[(\sqrt{r^2 - R_1^2}/R_1)|v_\theta| - v_r\right] \tag{10}$$

where H is the Heaviside step function,

$$J_{1,2} = \int_{v_r < 0, v_r > 0} \mathrm{d}\boldsymbol{v} v_r f(R_{1,2}, \boldsymbol{v})$$

$$M_i[\boldsymbol{v}(R_i)] = \frac{1}{2\pi k^2 T_i^2}\exp\left(-\frac{v_r^2 + v_\theta^2 + \Omega_i^2 R_i^2 - 2v_\theta r\Omega_i + v_z^2}{2kT_i}\right)$$

Particles from the internal cylinder arrive at point $P(r, \boldsymbol{v})$ if $\alpha = \tan^{-1}(v_\theta/v_r)$ is restricted to the interval $[-\bar{\alpha}, \bar{\alpha}]$, where $\tan\bar{\alpha} =$

$\sqrt{(r^2 - R_1^2)}/R_1$. The distribution function for v outside of the previous cone corresponds to the one of the molecules that is reemitted from R_2.

For the mass flux across each boundary to be zero,

$$-J_1 = J_2 \exp\left[-\frac{\Omega_2^2(R_2^2 - R_1^2)}{2kT}\right]$$

and J_2 is determined by the normalization condition

$$\int_{R_1}^{R_2} \mathrm{d}v r\, \mathrm{d}r f = m = \text{const}$$

From Eq. (10) we can evaluate the macroscopic variables and their fluxes as, for example,

$$p_{r\theta} = \int \mathrm{d}v v_r (v_\theta - u_\theta) f$$

$$= J_2 \exp\left[-\frac{\Omega_2^2(R_2^2 - R_1^2)}{2kT}\right] \frac{R_1^3}{r^2}(\Omega_1 - \Omega_2)$$

Subsequently, a linearized BGK model of Eq. (1) was considered, to take into account the effect of the collisions to first order. In particular for $T_1 = T_2 = T$, $\Omega_2 = 0$, and Ω_1 small, one takes $f = f_{eq}(1 + \phi)$ with $f_{eq} = [n_0/(2\pi kT)^{3/2}] \exp(-v^2/2kT)$ and where

$$D\phi = \nu\left[n^1 + \frac{v_\theta}{kT}u^1 + \left(\frac{v^2}{2kT} - \frac{3}{2}\right)\frac{T^1}{T} - \phi\right]$$

$$\phi(R_1, \boldsymbol{v}) = \frac{v_\theta}{kT}\Omega_1 R_1, \qquad v_r > 0$$

$$\phi(R_2, \boldsymbol{v}) = 0, \qquad v_r < 0 \tag{11}$$

where ν is the collision frequency,

$$n_0 u^1 = \int \mathrm{d}v v_\theta f_{eq}\phi, \qquad n^1 = \int \mathrm{d}v f_{eq}\phi$$

$$\frac{3}{2}n_0 k T^1 = \frac{1}{2}\int \mathrm{d}v v^2 f_{eq}\phi - \frac{3}{2}n_1 kT$$

The FMF solution ($\nu = 0$) is

$$\phi^{fm}(r, \boldsymbol{v}) = (v_\theta r/kT)\Omega_1 H\left[v_r - (\sqrt{r^2 - R_1^2}/R_1)|v_\theta|\right] \tag{12}$$

Substituting Eq. (12) into the right-hand side of Eq. (11) gives the first-order correction to the free molecular distribution function

$$\phi^1(r, \boldsymbol{v}) = \int_{R_1}^{r} \mathrm{d}r' \frac{\nu}{v_r(r')}\left\{\frac{v_\theta(r')}{kT}u^{1,fm}(r') - \phi^{fm}[r', \boldsymbol{v}(r')]\right\}$$

$$\times H\left(v_r - \frac{\sqrt{r^2 - R_1^2}}{R_1}|v_\theta|\right) - \int_{r}^{R_2} \mathrm{d}r' \frac{\nu}{v_r(r')}\left\{\frac{v_\theta(r')}{kT}u^{1,fm}(r')\right.$$

$$\left. - \phi^{fm}[r', \boldsymbol{v}(r')]\right\} H\left(\frac{\sqrt{r^2 - R_1^2}}{R_1}|v_\theta| - v_r\right) \tag{13}$$

(Note that $n^{1,fm} = 0$ and $T^{1,fm} = 0$.)

For the sake of simplicity, we assume $\nu = |v_r|/\lambda_0$, as is often done, although this assumption correctly holds for Ma_0 around unity. The macroscopic variables can be then explicitly evaluated and, therefore,

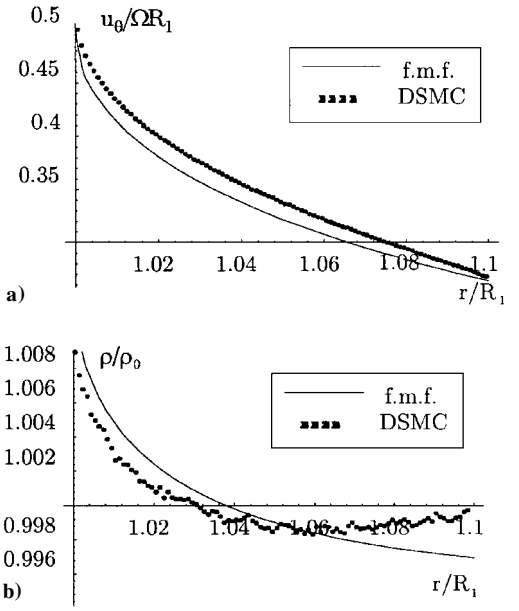

Fig. 4 Comparison of DSMC results with the analytical FMF results: $\Theta = 1$, $Kn_0 = 2$, $Ma_1 = 0.5$, $Ma_2 = 0$, and $Gr = 0.1$.

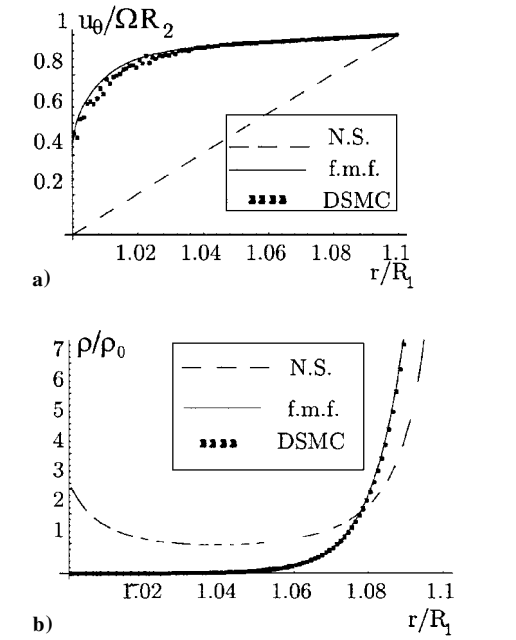

Fig. 5 Comparison of DSMC results with the results for NS and FMF: $\Theta = 1$, $Kn_0 = 0.2$, $Ma_1 = 0$, $Ma_2 = 8$, and $Gr = 0.1$.

$$u_\theta(R_1) = \frac{\Omega_1 R_1}{2} + \frac{1}{\lambda_0}\left[\frac{\Omega_1 R_1(R_2 - R_1)}{4} - \frac{\Omega_1 R_1}{4kT\sqrt{2\pi kT}}\int_{R_1}^{R_2} \mathrm{d}r\right.$$

$$\left. \times \int \mathrm{d}v_\theta v_\theta^2 \exp\left(-\frac{v_\theta^2}{2kT}\right) \mathrm{erf}\left(\frac{\sqrt{r^2 - R_1^2}|v_\theta|}{R_1\sqrt{2kT}}\right)\right]$$

and analogous this is for $u_\theta(R_2)$. The linearized BGK model provides calculated solutions that give negligible improvements with respect to the nonlinear FMF solutions, within an acceptable validity range of the simplifying assumptions.

Figure 4 shows the behavior of the mean velocity and of the density from Eq. (10) in comparison with the DSMC solutions. Moreover for small Kn_0 but great Ma_1 and/or Ma_2, we note that the macroscopic quantities of the gas behave as for the FMF (Figs. 5a and 5b). The same behavior (not shown) appears for small Knudsen number Kn_0, Ma_1, and Ma_2 but great Gr. Even better results

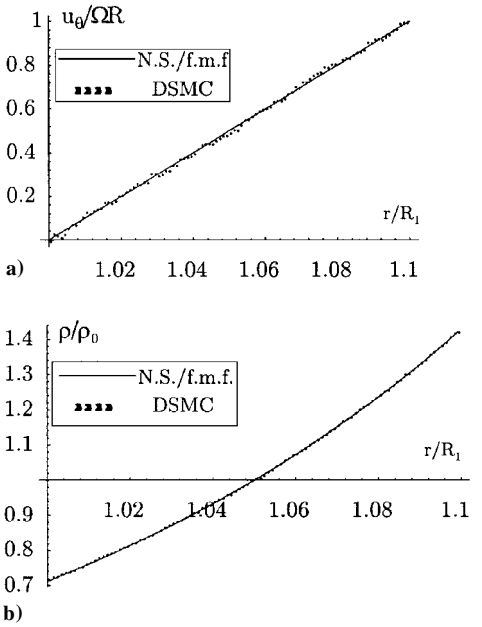

Fig. 6 Comparison of DSMC results with the results for NS and FMF; walls at the same angular speed Ω: $\Theta = 1$, $Kn_0 = 1$, $Ma_1 = 2$, and $Gr = 0.1$.

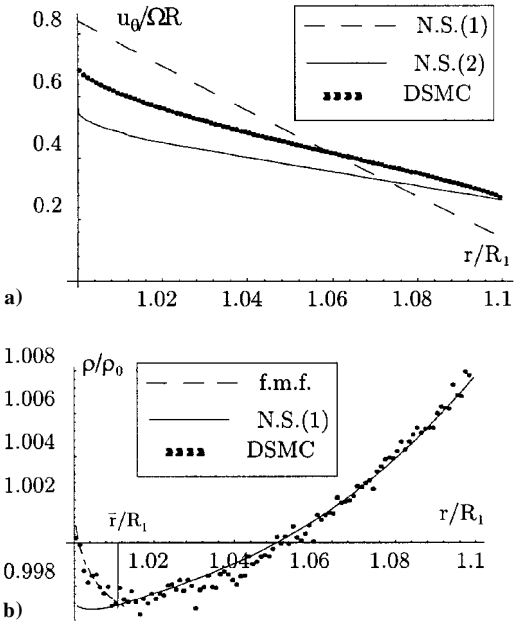

Fig. 7 Comparison of DSMC results with the results for NS and FMF; transition regime: $\Theta = 1$, $Kn_0 = 0.2$, $Ma_1 = 0.5$, $Ma_2 = 0$, and $Gr = 0.1$.

could be, of course, obtained by increasing the number of simulated particles.

If the cylinders are at the same temperature T and move with the same angular velocity Ω the free molecular distribution function is

$$f = \frac{n_0}{(2\pi kT)^{\frac{3}{2}}} \exp\left[-\frac{\Omega^2(R_1^2 - r^2)}{2kT}\right] \times \exp\left\{-\frac{\left[v_r^2 + (v_\theta - \Omega r)^2 + v_z^2\right]}{2kT}\right\} \tag{14}$$

which is also the solution of the Boltzmann equation (1) for any Knudsen number Kn_0.

As a consequence, the distribution of the macroscopic variables along r will be the same in the whole range of Knudsen number Kn_0 from the FMF to the hydrodynamic limit.

A further proof of this is obtained by observing Figs. 6a and 6b, where the FMF solution of Eq. (10), the NS solution from Eq. (3), and the results of the numerical simulations all fall on the same curve. This apparently trivial solution in a nontrivial system would mean, according to a reviewer's comment, that the distribution of flow properties is evidently determined entirely by inertial effects and the presence or absence of intermolecular collisions is of no consequence.

Note that, as already mentioned, constant values of μ and κ with T have been assumed in all NS calculations. This assumption is not quite correct at high Mach numbers at the walls, as in the case of Fig. 5. However, in that case, where high T and high T gradients are present in a layer close to the internal wall, whereas most of the particles migrate toward the external wall, the NS model no longer holds. The relative NS solutions in Fig. 5 are reported for reference.

Transition Regime

We have seen that the NS model subjected to the usual first-order slip conditions correctly describes the flow characteristics for $\Theta = 1$ and $Gr = 0.1$, and for $Ma_1 < 1$, $Ma_2 < 1$ provided that $Kn_0 \ll 1$. On the other hand, when $\Theta = 1$, $Gr \geq 0.1$, Ma_1 and/or $Ma_2 \gg 1$, the FMF model shows excellent agreement with the exact data for $Kn_0 < 1$. The same agreement can be realized $\forall(Ma_1, Ma_2)$ when $Kn_0 > 1$. Finally, we recall that for $\Omega_1 = \Omega_2$ and $\Theta = 1$, the FMF solution is the exact solution to the Boltzmann equation for any Knudsen number Kn_0.

One of the motivations for studying the Couette flow between cylinders was the initial assumption that the great variation of the Knudsen number distribution along r, under the effect of great centrifugal forces, might help a domain-separation-based investigation of the flow characteristics. Such a procedure would have been in line with the solutions obtained in Ref. 13, where the annulus is approximated as a strip between parallel straight lines and a force is imposed to simulate the centrifugal external force. However, this approach failed in our cases because one of the two limit models discussed before proved to be fairly satisfactory in all of those situations where the Knudsen number presents great variations.

On the other hand, a thorough investigation of the simulated experiments showed that, for Knudsen number Kn_0 assuming values that are usually considered as pertaining to the transition regime, and for $Ma_2 = 0$, $Ma_1 \ll 1$, $Gr \leq 0.1$, the flow in the annulus can be divided in two subdomains where the mass density follows different trends, although the local Knudsen number presents little variations along r. In particular, the density decreases with r in a region adjacent to the internal wall, whereas the increasing trend predicted by the continuum model is present in the rest of the field.

If we take, for example, the case in Fig. 7b, the FMF solution and the continuum solution intersect at a point $\bar{r}_0$ where the DSMC results show that a minimum value of ρ is present. We recall that the FMF solution for f and, consequently, for ρ depends on the constant J_2, that is, on the total mass m between the walls. Analogously, the ρ distribution predicted by the NS equation depends on m. Then point $\bar{r}$, such that the total mass in the annulus is conserved, can be evaluated. Point $\bar{r}$ can be considered as a zeroth-order approximation of a fictitious boundary between the continuous region and the rarefied region.

In all cases similar to the one we are discussing, one can realize that a linear tangential velocity distribution, as predicted by the linear slip flow NS model, is present in a great part of the annular region, whereas the rate of change of u_θ is not satisfactorily evaluated. This can be attributed to the boundary conditions not being correctly imposed.

In the transition regime, Eqs. (7) do not provide an accurate evaluation of the velocity slip Δ at the walls, $\Delta_1 = [u_\theta(R_1) - \Omega_1 R_1]/(\Omega_1 R_1)$ and $\Delta_2 = [u_\theta(R_2) - \Omega_2 R_2]/(\Omega_1 R_1)$. Of course, Δ_1 and Δ_2 fall in a range from zero (no slip) to the FMF solution value. In Tables 1–3 we present a few calculations relative to the velocity slip at the wall from DSMC (Δ^{MC}), linear continuum theory (Δ^{NS}), and FMF (Δ^{FMF}) in the extremes of the Knudsen number Kn_0 range. For $Kn_0 \to 0$, Δ increases linearly with Kn_0, whereas Δ achieves

Table 1 Velocity slip calculations: $\Theta = 1$, $Ma_1 = 0.5$, $Gr = 0.1$, and $Kn_0 = 0.2$

DSMC	FMF	NS
$\Delta_1^{MC} = -0.32$	$\Delta_1^{FMF} = -0.50$	$\Delta_1^{NS} = -0.16$
$\Delta_2^{MC} = 0.27$	$\Delta_2^{FMF} = 0.27$	$\Delta_2^{NS} = 0.13$

Table 2 Velocity slip calculations: $\Theta = 1$, $Ma_1 = 0.5$, $Gr = 0.05$, and $Kn_0 = 0.2$

DSMC	FMF	NS
$\Delta_1^{MC} = -0.32$	$\Delta_1^{FMF} = -0.50$	$\Delta_1^{NS} = -0.16$
$\Delta_2^{MC} = 0.29$	$\Delta_2^{FMF} = 0.32$	$\Delta_2^{NS} = 0.14$

Table 3 Velocity slip calculations: $\Theta = 1$, $Ma_1 = 0.5$, $Gr = 0.05$, and $Kn_0 = 0.8$

DSMC	FMF	NS
$\Delta_1^{MC} = -0.42$	$\Delta_1^{FMF} = -0.50$	$\Delta_1^{NS} = -0.16$
$\Delta_2^{MC} = 0.34$	$\Delta_2^{FMF} = 0.27$	$\Delta_2^{NS} = 0.13$

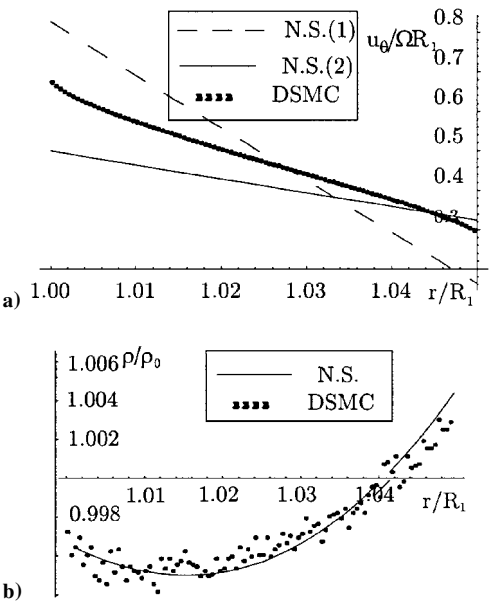

Fig. 8 Comparison of DSMC results with the results for NS and FMF; transition regime: $\Theta = 1$, $Kn_0 = 0.2$, $Ma_1 = 0.5$, $Ma_2 = 0$, and $Gr = 0.05$.

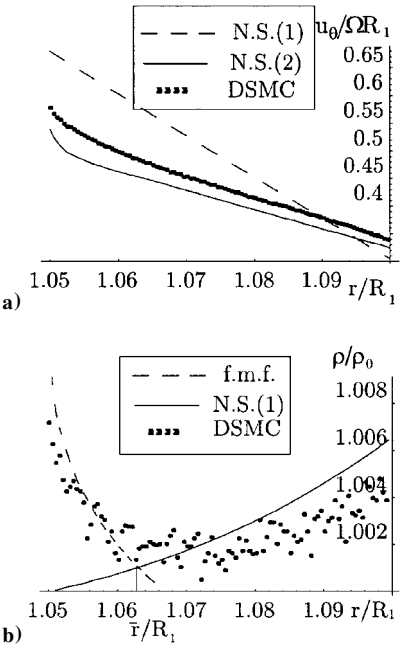

Fig. 9 Comparison of DSMC results with the results for NS and FMF; transition regime: $\Theta = 1$, $Kn_0 = 0.8$, $Ma_1 = 0.5$, $Ma_2 = 0$, and $Gr = 0.05$.

its maximum value Δ_{max} and is proportional to Kn_0^{-1} as $Kn_0 \to \infty$. As an example, at $Kn_0 = 0.8$, Δ is already well approximated by its maximum free molecular value. We can then assume, for the cases under consideration, that the exact Δ value is satisfactorily approximated by $\Delta_{max} = \Delta^{FMF}$ in the range $0.1 \leq Kn_0 \leq 1$.

In any case, the parameter of most interest in rarefied gasdynamics is the Knudsen number and Tables 2 and 3 show the great influence of Knudsen number Kn_0 on the wall slip. However, the lesser influence of Gr is also considered because it may assume relevance in applications related to centrifuges.

We can now contruct a solution in a particular situation such as the one in Fig. 7a, where the NS(1) velocity profile with linear slip boundary condition BC is practically linear with r almost everywhere.

First $\Delta_{1,max}$ and $\Delta_{2,max}$ are taken as limits to the slip values and the NS solution provides $u_\theta(\bar{r})$. The velocity profile between R_1 and $\bar{r}$ is then recalculated by the FMF solution with the updated BC. The proposed procedure was applied in a number of cases such as the one in Figs. 7a and 7b. Further results are shown in Figs. 8 and 9, which show the influence of Gr and Knudsen number Kn_0 on the solution. As mentioned, in these cases the density across the gap is almost constant. Note in Fig. 8b how good the NS calculated density distribution is, whereas the NS velocity profile needs the FMF BC to approximate the exact data. Comparison of Figs. 7 and 8 show that an increased gap moves $\bar{r}$ toward the external wall. Furthermore, Figs. 8 and 9 show the increased rarefaction effects due to an increased Knudsen number Kn_0.

Recently the effects of temperature difference between the walls and of a condensation have been considered following a numerical approach and a BGK approximation.[13,14] We carried out a few simulations for $\Theta \neq 1$, and the influence of the temperature parameter on the field configuration in the transition regime proved to be very significant. An investigation on these effects is beyond the scope of this presentation and is left to a forthcoming paper.

Conclusion

Couette flow between concentric cylinders has heretofore been a reference problem in rarefied gasdynamics as proven by the continuing recent literature.[13,14] One deals with a mathematical model of a physically interesting situation where mass forces can play a dominant role. In spite of the simplicity of the model when described either by the Boltzmann equation or by simpler models, exact and even approximate analytic solutions are missing for the general case. This is the case for the one-dimensional problem, not to speak of two- and three-dimensional macroscopic effects that may arise in a unstable situation. A great number of numerical approaches have been proposed, the latest one being the direct simulation based on a MonteCarlo procedure. In this framework, the present paper has reconsidered the problem with all of its limitations and in the whole range of Knudsen numbers.

After validating the computational code against the analytic solutions for the two extreme regimes of continuous flow and FMF, the results of the direct simulations were taken as exact references to evaluate the accuracy of a solution procedure for cases of transitional flow where, in spite of the centrifugal effects, the density in the annular region is practically constant. It has been proven that the physical intuition that centrifugal force moves all of the gas toward the external wall must be carefully considered. An analytic solution for a linearized BGK model has been presented for a case where only the numerical results were known, following a variational approach.[1]

Acknowledgments

This work was partially supported by the Italian Space Agency through Contract ARS-96-15 and by the Italian National Research Council CNR-GNFM.

References

[1]Cercignani, C., and Sernagiotto F., "Cylindrical Couette Flow of a Rarefied Gas," *Physics of Fluids*, Vol. 10, No. 6, 1967, pp. 1200–1204.

[2]Alofs, D. J., and Springer, R. W., "Cylindrical Couette Flow Experiments in the Transition Regime," *Physics of Fluids*, Vol. 14, No. 2, 1971, pp. 298–305.

[3]Sharipov, F. M., and Kremer, G. M., "Nonlinear Couette Flow Between Two Rotating Cylinders," *Transport Theory Statistical Physics*, Vol. 25, No. 2, 1996, pp. 217–229.

[4]Makihara, M., and Ito, T., " Numerical Analysis of Rarefied Cylindrical Couette Flows," *Proceedings of the 14th International Symposium on RGD*, edited by H. Oguchi, Vol. 1, Univ. of Tokyo Press, Tokyo, 1983, pp. 159–166.

[5]Nanbu, K., "Analysis of Cylindrical Couette Flows by Use of the Direct Simulation Method," *Physics of Fluids*, Vol. 27, No. 11, 1984, pp. 2632–2635.

[6]Schamberg, R., "The Fundamental Differential Equations and the Boundary Conditions for High Speed Slip-Flow and Their Application to Several Specific Problems," Ph.D. Dissertation, Aerospace Dept., California Inst. of Technology, Pasadena, CA, 1947.

[7]Wood, L. C., *An Introduction to the Kinetic Theory of Gases and Magnetoplasmas*, Oxford Univ. Press, Oxford, 1993, pp. 178–181.

[8]Bird, G. A., "Molecular Gas Dynamics and the Direct Simulation of Gas Flows," Clarendon, Oxford, 1994, pp. 218–220, 408–416.

[9]Bardos, C., Caflish, R. E., and Nicolaenko, B., "Thermal Layer Solution for the Boltzmann Equation," *Statistical Physics and Dynamical System*, edited by J. Fritz, A. Jaffe, and J. L. Lebowitz, Vol. 10, Progress in Physics, Birkhäuser, Boston, 1985, pp. 235–252.

[10]Esposito, R., Lebowitz, J. L., and Marra, R., "The Navier–Stokes Limit of the Stationary Solution of the Nonlinear Boltzmann Equation," *Journal of Statistical Physics*, Vol. 78, No. 1–2, 1995, pp. 382–412.

[11]Cercignani, C., *The Boltzmann Equation and Its Applications*, Springer–Verlag, New York, 1988, pp. 254, 255.

[12]Sone, Y., "Asymptotic Theory of Flow of Rarefied Gas over a Smooth Boundary I," *Proceedings of the 6th International Congress on RGD*, edited by L. Trilling and H. Y. Wachman, Vol. 1, Academic, New York, 1969, pp. 243–253.

[13]Johnson, E. A., and Stopford, P. J., "Shear Flow in the Presence of 'Strong Rotation': II. Approximation for Continuum-Plus-Rarefied Flow," *Journal of Physics D: Applied Physics*, Vol. 16, 1983, pp. 1207–1215.

[14]Gramani Cumin, L. M., Sharipov, F. M., and Kremer, G. M., "Rarefied Gas Flow Between Two Cylinders Caused by the Evaporation and Condensation on their Surfaces," *Physics of Fluids*, Vol. 10, No. 12, 1998, pp. 3203–3208.